SUPPLEMENTARY INFORMATION

Studying Localized Corrosion using Liquid Cell Transmission Electron Microscopy

See Wee Chee[1], Sarah H. Pratt[2], Khalid Hattar[2], David Duquette[1], Frances M. Ross[3], and Robert Hull[1]

[1] Department of Materials Science and Engineering, Rensselaer Polytechnic Institute, Troy, NY 12180

[2] Sandia National Laboratories, Albuquerque, NM 87123

[3] IBM T. J. Watson Research Center, Yorktown Heights, NY 10598

List of Contents

Methods and Materials

The corrosion of copper (Cu) and aluminum (Al) was examined using two different liquid cell systems. In each case, a thin polycrystalline film of the metal was deposited directly on one of the two window chips of a liquid cell. A plain silicon nitride (SiN) window chip was used on the other side. The rectangular SiN window was 50 nm thick with edge dimensions ranging from 50–200 μm. For studies of Cu,

polycrystalline films were deposited to a thickness of 50 nm using pulsed laser deposition (PLD). The PLD films were deposited using a KrF laser with a wavelength of 248 nm, 34 ns full width at half-maximum, and an energy density of 1-2 J m^{-2}. The target and substrate were at a base vacuum of 2.7 x 10^{-5} Pa. A pulse repetition of 35 Hz was continued until the desired nominal thicknesses For Al, 30 nm films deposited by PLD and 100 nm films deposited using electron beam evaporation were examined. Using Millipore water and scientific grade solid sodium chloride, aqueous NaCl solutions (0.01–6 M) were made and introduced into the cells during observation. The PLD Cu and Al film systems were imaged using a Protochips Poseidon 200 Liquid Flow Holder (Protochips Inc, Rayleigh, NC, USA) in a JEOL 2100 LaB_6 TEM (JEOL Ltd., Tokyo, Japan). In this case, 150 nm thick, patterned Au films were used to control the spacing between the two window chips. The evaporated Al films were examined in a Hummingbird Scientific Liquid Flow Holder (Hummingbird Scientific, Lacey, WA, USA) in a JEOL 2011 LaB_6 TEM. In this case, 0.96 μm polystyrene spheres were used as spacers between the top and bottom chips. Corrosion experiments under potentiostatic control were performed in the Hummingbird Scientific Liquid Flow Holder with biasing capability. The Al films were also deposited using by electron beam evaporation. A potential was applied to the thin film sample using metal contacts that touched the chip along one of its edges. There were three metal leads and the chip was selectively masked during deposition to allow only one to touch the film. The other two leads, which were also exposed to the solution, were used as reference and working electrodes respectively. The potential was controlled using a Gamry Interface 1000 potentiostat (Gamry Instruments, Warminster, PA, USA). 500 nm spacers were used between chips in these experiments. The focused ion beam patterned films were made by first depositing the 100 nm Al film and then implanting the Al with Au ions at 30 keV using an Orsay Physics mass-separated focused ion beam column (Orsay Physics, France). The ions were implanted as an array of spots with a dose of 1 x 10^7 ions per spot and a spot to spot separation of 5 μm.

Experimental Considerations for Liquid Cell Corrosion Studies

Many experimental parameters can be varied in a liquid cell TEM experiment and the considerations relevant to corrosion studies are discussed here.

1. Sample geometry and thickness

A key constraint for liquid cell electron microscopy is the requirement for electron transparency. This means that the total thickness of the sample can only be on the order of a few hundred nanometers to preserve reasonable image resolution[1], depending on the density of the material under study. Conventional samples may be mechanically prepared or thinned using a focused ion beam (FIB). Such samples had been used for corrosion studies in gaseous environments (for example corrosion of an AA2024-T3 alloy was examined by Malladi *et al.*[2–4]). However, for experiments with a liquid environment, the sample thickness includes the windows, liquid and material of interest. This thickness constraint limits aqueous corrosion studies to thin films and nanoscale powders and particles. Metal thin films formed by physical vapor deposition on one surface of the liquid cell, as the experiments presented in the paper, have two benefits for *in situ* corrosion studies. First, contamination and sample preparation artifacts are minimized. Second, the corrosion of thin films is a relatively well studied system in corrosion science[5], allowing us to compare the observations from this new technique with known corrosion behavior and mechanisms. To expand the range of *in situ* corrosion studies, we can pattern the thin films to include junctions between dissimilar metals. However, thin film samples still remain a small subset of the materials of interest in corrosion science. Recent experiments on battery materials have demonstrated the feasibility of cutting thin sections with a gallium focused ion beam (FIB) and welding these sections using ion beam induced deposition of Pt on the pre-patterned electrodes in the liquid cell[6–8]. This approach allows sections from bulk samples to be examined, thereby increasing the opportunities for *in situ* experiments to answer key questions on corrosion in more general systems. It should be noted that corrosion can be sensitive to the surface chemistry of the specimen. The degree to which Ga^+-ion

implantation artifacts arising from FIB specimen preparation can be controlled remains to be determined.

2. The liquid: compatibility, chemistry, and surface wettability

As a practical consideration, it is clearly important to make sure that any liquid used is compatible with the different materials that make up the microfluidic cell and specimen holder. These include the materials comprising the holder body, the microchips, and any o-rings or bonding agents used to make the hermetic seal. Compatibility is particularly important in corrosion studies due to the reactive nature of many liquids of interest. Solvents that can swell the o-rings or dissolve the bonding agents should clearly be avoided or used with care. Liquids that corrode the holder material or silicon nitride membranes at a high rate (relative to the duration of an experiment) can be detrimental to the vacuum integrity while the holder is in the microscope. Factors that affect metal dissolution rates include solution concentration, pH, and liquid temperature. But even slow reactions with the holder material, SiN membranes, bonding agents or o-rings can lead to artifacts, as dissolved species may change the chemistry of the solution and affect the corrosion process under study. In this context, it is important to note that small changes in solution chemistry have a significant effect on corrosion. To obtain reproducible results, a consistent experimental procedure is desirable. For example, aqueous solutions can be de-aerated by bubbling inert gases such as nitrogen or argon before loading into the syringe pump, while ionic liquids that are sensitive to water generally have to be loaded into the liquid cell in a glove box [8]. Finally, we note that while the NaCl solutions used here are benign, general precautions must be taken to protect the TEM operator from accidental exposure and to ensure safe disposal of the liquid outlet stream if hazardous liquids are used.

A second consideration related to the liquid is its wettability on the interior surfaces of the liquid cell. SiN membrane window chips are usually hydrophobic as-manufactured, with the hydrophobicity commonly attributed to surface contaminants. A hydrophobic surface is undesirable because of the increased likelihood that the liquid layer will de-wet within the cell. Plasma cleaning or glow discharge treatments

are typically used to render the surface hydrophilic[9]. However, in the experiments described here, one of the SiN surfaces is covered by the metal film and this may have different wetting characteristics. Furthermore, the wetting behavior of aqueous solutions can also change with solute concentration. For example, we find that liquid cells become more difficult to wet as the NaCl concentration is increased. Two ways to mitigate this issue are to pre-wet the cell with the liquid or use a surface treatment to render the metal film surface hydrophilic. Pre-wetting can be carried out with liquids that do not corrode the sample, such as deionized water. Alcohols such as ethanol were also found to be useful for pre-wetting because the liquid cell can be assembled dry and pre-loaded into the TEM, allowing for pre-inspection of the sample. Ethanol easily wicks into the dry cell (presumably due to its lower surface tension) after it is introduced *via* the fluid tubing, priming the cell for the subsequent introduction of aqueous solutions. However, the use of ethanol leads to a side effect of increased carbon contamination under the electron beam. The alternative approach of pre-treating the metal film to render it hydrophilic can be useful provided the treatment does not interfere with subsequent corrosion reactions. For example, treatment with Alcian blue, a polyvalent basic dye, has been found to render the SiN surface hydrophilic[10] and may also be useful for treating metal films.

3. Electrochemical experiments and film geometry

Significant challenges remain in developing the liquid cell TEM (LCTEM) technique to definitively answer the most important questions regarding corrosion processes: what determines the location of pit initiation, and how do pits grow in the early stages? As we have shown, an effective way to initiate the formation of a pit is to potentiostatically bias the sample to near its pitting potential. However, existing electrochemical cells for *in situ* TEM experiments are not specifically designed for corrosion studies. The crucial difference between a corrosion experiment and an electrochemical experiment involving electrodeposition or battery charging is that, in the latter, the reaction takes place at a well-defined interface, such as the edge of a patterned electrode. Masking the metal film or covering the surface can restrict the corrosion to areas near the electron-transparent window and increase the likelihood that a pit

will form in the observation window. A second difficulty with imaging corrosion processes is that the dissolution of existing material is being observed, so that significant contrast variation is only expected when the film is perforated, given the relatively large total sample thickness. As such, extending liquid cell transmission electron microscopy to study corrosion may require re-evaluation of electrode materials, electrode patterns, spacer layers, and electrode to sample geometries, with additional consideration given to the issue of galvanic coupling described in the next section.

4. Galvanic corrosion between metal and microfluidic cell materials

In microfluidic liquid cells, gold and platinum are commonly used to form spacers or electrodes because of their inertness. However, these materials can cause difficulties in corrosion experiments. Contact between an active metal such as aluminum and these noble metals can give rise to galvanic corrosion of the active metal. In Figure S1(a) we show an example of this. After immersion in a 0.01 M NaCl solution, dissolution is clearly visible in Al squares that make contact with Au, whereas isolated Al squares on bare SiN remain largely intact. Al films deposited on microchips with Au spacers also show rapid dissolution in both de-ionized water and saturated salt solutions (Figure S1(b)). This effect needs to be considered in optimizing chip contact and spacer design.

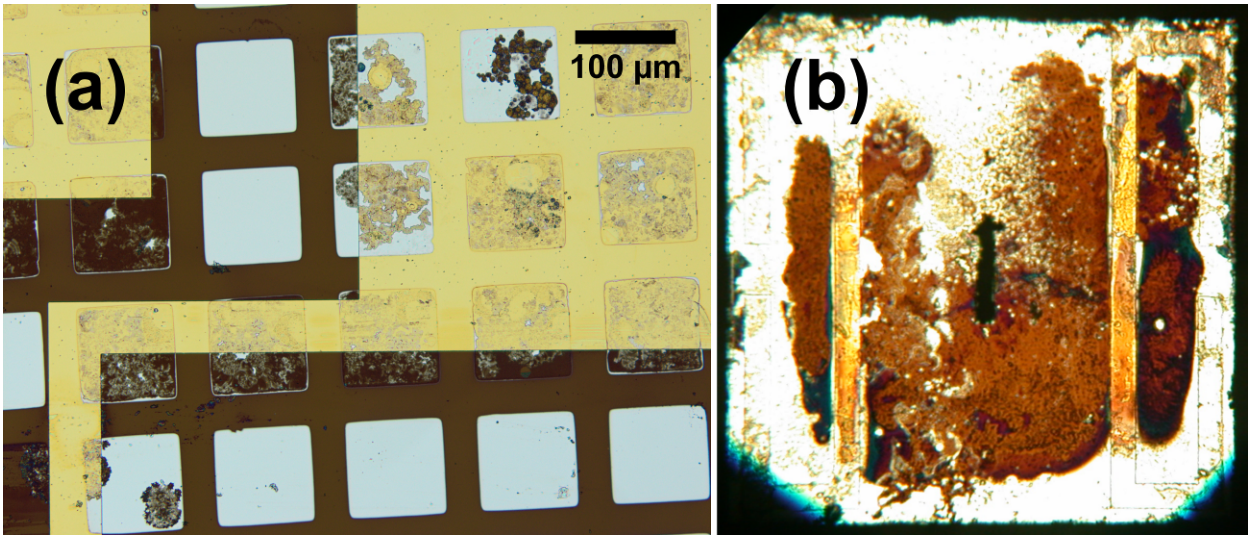

Figure S1. (a) Light microscope image of a 100 nm thick Al thin film (deposited by electron beam evaporation) in 100 um squares patterns produced with a shadow mask on a biasing chip containing Au electrodes. The sample was exposed to 0.01 M NaCl solution for 4 hours. The squares in contact with Au show significant corrosion relative to the squares that are isolated. (b) Dissolution of 30 nm Al thin film in deionized water possibly caused by galvanic corrosion due to the Au spacers on the chip.

5. Imaging Conditions

Both TEM and scanning transmission electron microscopy (STEM) have been used in liquid cell TEM imaging. In general, STEM has the advantage of being able to image through a wider spacer distance between the windows surrounding liquid, whereas TEM offers higher frame rates in imaging[11]. It is obvious that both the resolution and image contrast are significantly degraded in electron microscopy when liquid is present in the cell, due to diffuse scattering of electrons by the liquid. Comparing micrographs of 100 nm thick Al thin films before and after the introduction of liquid (Figure S2 (a) and (b)), it can be seen that the clearly defined grain structure of the sample is degraded to a set of relatively poorly defined grains with only strongly diffracting grains showing good contrast. Furthermore, even if relatively small spacers are used to separate the two windows, the SiN membranes bow from the pressure differential between the column vacuum and the inside of the cell resulting is a bulging of the windows and subsequent thicker layer of fluid near the center of the window. The progressive reduction in image quality as the thickness of the liquid layer increases from the corner of the viewing window towards the center can also be seen in Figure S2 (b). On the other hand, the liquid layer cannot be too thin, otherwise the experiment will not be representative of the phenomenon under study. The ability to resolve fine scale initial localized corrosion events, such as pit nucleation, must be balanced against the need to maintain a liquid layer that is thick enough for processes such as diffusion in the liquid to be representative of "bulk" configurations. Figure S2 (c) and (d) are images of 50 nm thick Cu thin films deposited with fine grain sizes using pulsed laser deposition. 150 nm thick Au spacers were used in this case, leading to an overall improvement in image quality. Other methods to improve image quality include inserting an objective

aperture, using energy filtering, or displacing the liquid by forming a gas bubble, which improves resolution and minimizes the dose needed for imaging [11].

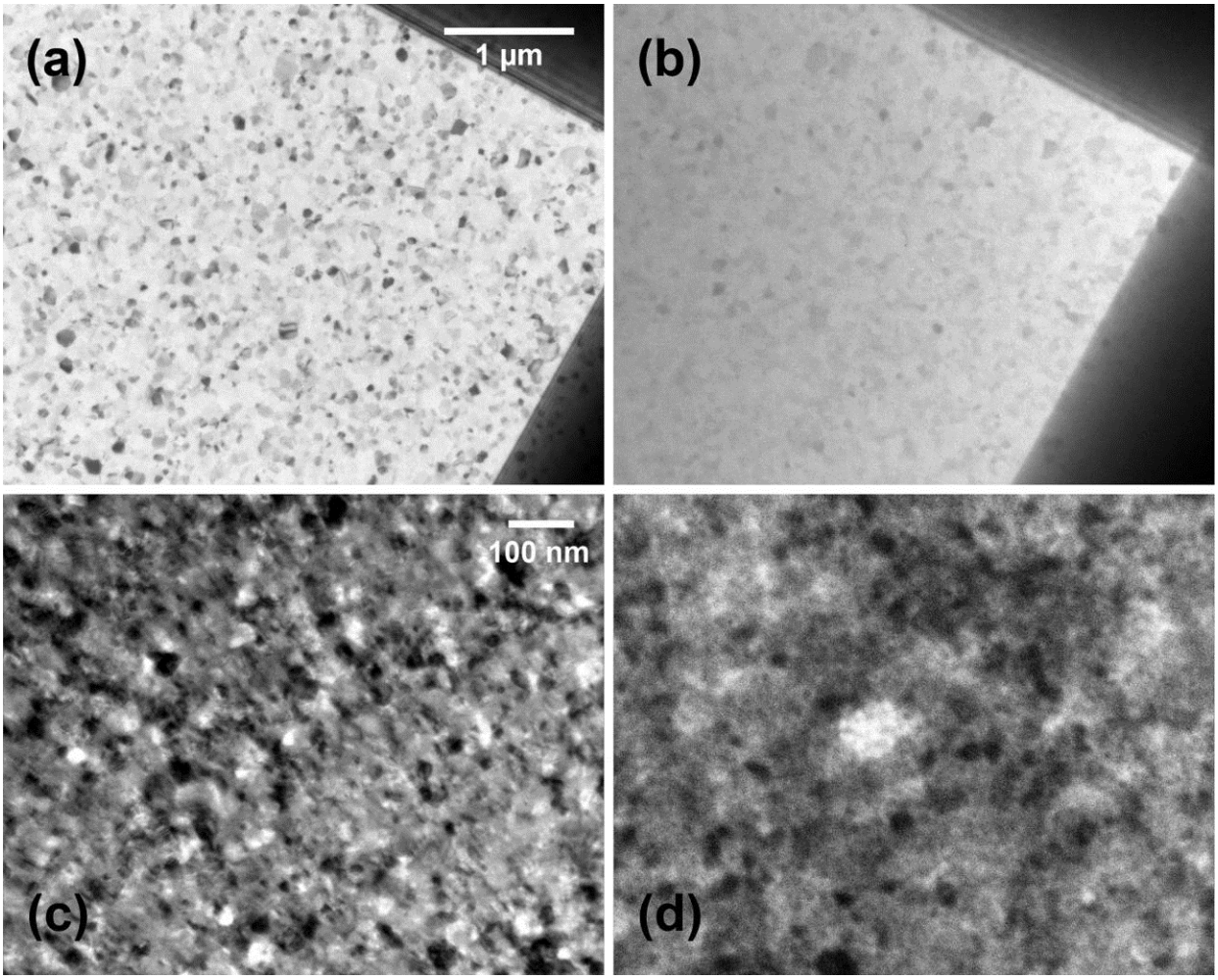

Figure S2. 100 nm Al thin films (a) before and (b) after the introduction of liquid. The spacers used are 0.96 μm polystyrene spheres. 50 nm Cu thin films (c) before and (d) after the introduction of liquid. The spacers are 150 nm Au films.

6. Electron beam effects

In every liquid cell experiment (as in *in situ* TEM experiments broadly), correct interpretation of results requires an understanding of the influence of the electron beam on the process under study. The most important effect of the beam is the generation of a cascade of species by radiolysis of water[12] while beam

heating is not considered significant for typical liquid cell imaging parameters. Radiolysis is critical as it creates highly reactive species, such as hydrated (solvated) electrons[13]. These species are thought to be responsible for the nucleation and growth of nanoparticles observed during irradiation of aqueous solutions containing metal ions[14–16]. Radiolysis also forms molecular hydrogen, plus molecular oxygen at a slower rate[12]. These gas molecules are thought to give rise to bubble formation during imaging[12]. The beam also has effects associated with conventional electron microscopy where irradiation can enhance the rate of surface contamination[9], although this can be reduced by plasma cleaning the chips prior to assembly and/or by using ultra-pure water. Strategies to minimize beam effects, based on the low-dose protocols developed for imaging biological materials, are currently being explored in the liquid cell community. For example, low dose imaging can reduce the formation rate of radiolytic hydrogen, keeping the hydrogen concentration below the solubility limit and allowing bubble-free imaging[12]. However, even low dose imaging produces a non-zero concentration of radiolysis species.

Given the sensitivity of corrosion processes to solution chemistry, the formation of radiolytic species may accelerate or modify the corrosion process in an irradiated area (see Figure S3). For NaCl solutions, experiments with ionizing radiation have shown that species $HClO^{\cdot -}$, $Cl^{\cdot}$, $Cl_2^{\cdot -}$ are formed by radiolysis[17], in addition to the species produced during radiolysis of pure water. $HClO^{\cdot -}$, for example, is known to yield chlorite and hypochlorite as reaction products and the latter can turn the alkaline NaCl solutions strongly oxidizing[18]. To model the concentrations of the radiolytic species generated during TEM observations, an approach has been developed[19] that uses empirical creation and reaction rates, extrapolated to the high dose rates associated with TEM (~10^6-10^{10} Gy/sec), and also includes the fact that species can diffuse out of the irradiated area[12]. Calculations that include the presence of Cl^- ions[20] show that, at typical TEM conditions (8x10^7 Gy/sec in our case), $HClO^{\cdot -}$ is formed at concentrations less than 100 μM. The simulations predict that this concentration should become stronger at higher initial Cl^- ion concentration or at higher dose rate. While it is likely that $HClO^{\cdot -}$ and other radiolytic species will affect the corrosion rate under the electron beam, the detailed nature of these beam induced effects remain

to be explored. However, the complexity of radiolysis effects makes it essential to compare liquid cell data with *ex situ* corrosion structures, and to examine fresh areas of the film in the liquid cell to compare with the area that received the highest dose. Such comparisons can help ensure that the liquid cell experiments provide the best possible model of corrosion processes that take place in larger volumes.

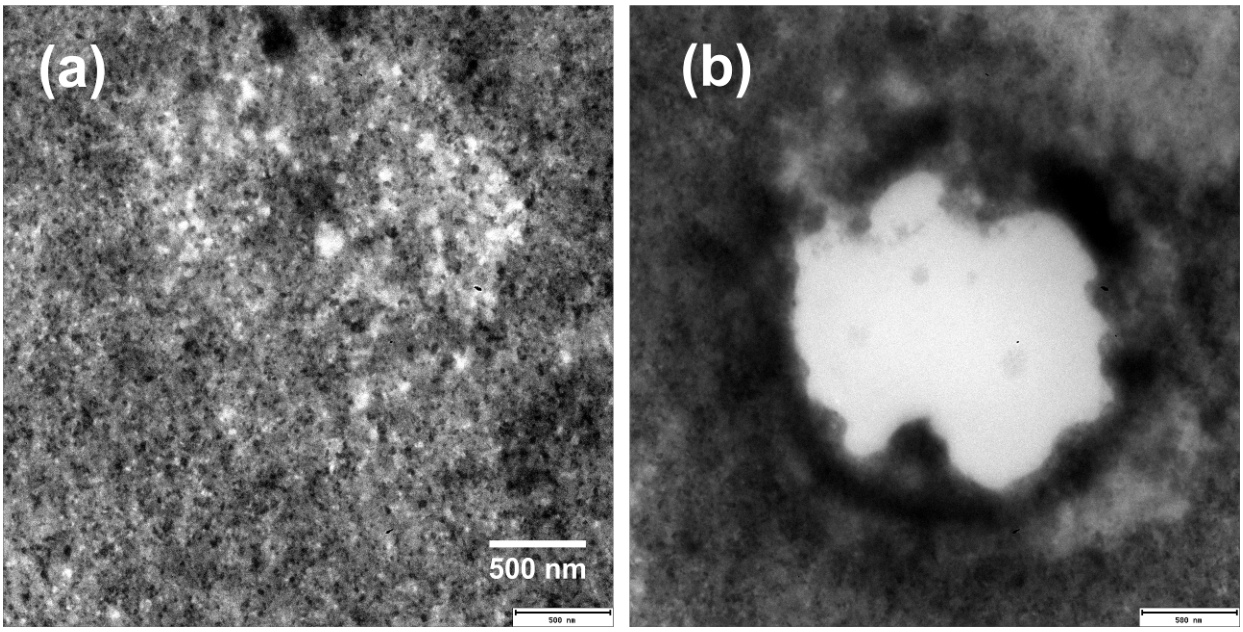

Figure S3. A comparison of the same Cu film area illustrating beam induced dissolution, (a) before and (b) after imaging at higher magnification for 10 seconds with a condensed beam.

References

1. N. de Jonge and F. M. Ross, *Nat. Nanotechnol.*, 2011, **6**, 695–704.

2. S. R. K. Malladi, Q. Xu, F. D. Tichelaar, H. W. Zandbergen, F. Hannour, J. M. C. Mol, and H. Terryn, *Surf. Interface Anal.*, 2012, **45**, 1619–1625.

3. S. R. K. Malladi, F. D. Tichelaar, Q. Xu, M. Y. Wu, H. Terryn, J. M. C. Mol, F. Hannour, and H. W. Zandbergen, *Corros. Sci.*, 2013, **69**, 221–225.

4. S. Malladi, C. Shen, Q. Xu, T. de Kruijff, E. Yücelen, F. Tichelaar, and H. Zandbergen, *Chem. Commun. (Camb).*, 2013, **49**, 10859–61.

5. G. Frankel, *J. Electrochem. Soc.*, 1998, **145**, 2186.

6. R. Unocic, L. Adamczyk, N. Dudney, D. Alsem, N. Salmon, and K. More, *Microsc. Microanal.*, 2011, **17**, 1564–1565.

7. M. Gu, L. R. Parent, B. L. Mehdi, R. R. Unocic, M. T. McDowell, R. L. Sacci, W. Xu, J. G. Connell, P. Xu, P. Abellan, X. Chen, Y. Zhang, D. E. Perea, J. E. Evans, L. J. Lauhon, J.-G. Zhang, J. Liu, N. D. Browning, Y. Cui, I. Arslan, and C.-M. Wang, *Nano Lett.*, 2013, **13**, 6106–6112.

8. B. Layla Mehdi, M. Gu, L. R. Parent, W. Xu, E. N. Nasybulin, X. Chen, R. R. Unocic, P. Xu, D. a Welch, P. Abellan, J.-G. Zhang, J. Liu, C.-M. Wang, I. Arslan, J. Evans, and N. D. Browning, *Microsc. Microanal.*, 2014, **20**, 484–92.

9. T. J. Woehl, K. L. Jungjohann, J. E. Evans, I. Arslan, W. D. Ristenpart, and N. D. Browning, *Ultramicroscopy*, 2013, **127**, 53–63.

10. S. M. Hoppe, D. Y. Sasaki, A. N. Kinghorn, and K. Hattar, *Langmuir*, 2013, **29**, 9958–61.

11. K. L. Klein, I. M. Anderson, and N. de Jonge, *J. Microsc.*, 2011, **242**, 117–23.

12. J. M. Grogan, N. M. Schneider, F. M. Ross, and H. H. Bau, *Nano Lett.*, 2013, **14**, 359–364.

13. M. S. Matheson, in *Solvated Electron*, 1965, vol. 39, pp. 45–54.

14. K. W. Noh, Y. Liu, L. Sun, and S. J. Dillon, *Ultramicroscopy*, 2012, **116**, 34–8.

15. T. J. Woehl, J. E. Evans, I. Arslan, W. D. Ristenpart, and N. D. Browning, *ACS Nano*, 2012, **6**, 8599–610.

16. P. Abellan, T. J. Woehl, L. R. Parent, N. D. Browning, J. E. Evans, and I. Arslan, *Chem. Commun. (Camb).*, 2014, **50**, 4873–80.

17. E. Atinault, V. De Waele, U. Schmidhammer, M. Fattahi, and M. Mostafavi, *Chem. Phys. Lett.*, 2008, **460**, 461–465.

18. M. Kelm, E. Bohnert, and I. Pashalidis, *Res. Chem. Intermed.*, 2001, **27**, 503–507.

19. N. M. Schneider, M. M. Norton, B. J. Mendel, J. M. Grogan, F. M. Ross, and H. H. Bau, *J. Phys. Chem. C*, 2014, **118**, 22373–22382.

20. J. H. Park, N. M. Schneider, J. M. Grogan, M. C. Reuter, H. H. Bau, S. Kodambaka, and F. M. Ross, Journal Article in Preparation.